International Journal of Radiation Oncology biology • physics

www.redjournal.org

Biology Contribution

Monitoring Tumor Response to Carbogen Breathing by Oxygen-Sensitive Magnetic Resonance Parameters to Predict the Outcome of Radiation Therapy: A Preclinical Study

Thanh-Trang Cao-Pham, BSc,* Ly-Binh-An Tran, PhD,* Florence Colliez, PhD,* Nicolas Joudiou, PhD,* Sabrina El Bachiri, PhD,† Vincent Grégoire, PhD,‡ Philippe Levêque, PhD,* Bernard Gallez, PhD,* and Bénédicte F. Jordan, PhD*

**Université Catholique de Louvain, Louvain Drug Research Institute, Biomedical Magnetic Resonance Research Group, Brussels, Belgium; †Université Catholique de Louvain, IMMAQ Technological Platform, Methodology and Statistical Support, Louvain-la-Neuve, Belgium; and ‡Université Catholique de Louvain, Institute of Experimental and Clinical Research, Center for Molecular Imaging, Radiotherapy and Oncology, Brussels, Belgium*

Received Oct 21, 2015, and in revised form Apr 25, 2016. Accepted for publication Apr 30, 2016.

Summary

This study compared R_1-related parameters and R_2* in assessing sensitivity to changes in tumor oxygenation and evaluated their potential as predictive markers for the outcome of radiation therapy (RT) in rat tumor models. At the intratumoral level, all magnetic resonance biomarkers successfully reflected the tumor

Purpose: In an effort to develop noninvasive in vivo methods for mapping tumor oxygenation, magnetic resonance (MR)-derived parameters are being considered, including global R_1, water R_1, lipids R_1, and R_2*. R_1 is sensitive to dissolved molecular oxygen, whereas R_2* is sensitive to blood oxygenation, detecting changes in dHb. This work compares global R_1, water R_1, lipids R_1, and R_2* with pO_2 assessed by electron paramagnetic resonance (EPR) oximetry, as potential markers of the outcome of radiation therapy (RT).
Methods and Materials: R_1, R_2*, and EPR were performed on rhabdomyosarcoma and 9L-glioma tumor models, under air and carbogen breathing conditions (95% O_2, 5% CO_2). Because the models demonstrated different radiosensitivity properties toward carbogen, a growth delay (GD) assay was performed on the rhabdomyosarcoma model and a tumor control dose 50% (TCD50) was performed on the 9L-glioma model.
Results: Magnetic resonance imaging oxygen-sensitive parameters detected the positive changes in oxygenation induced by carbogen within tumors. No consistent correlation

Reprint requests to: Bénédicte F. Jordan, PhD, Biomedical Magnetic Resonance Group (REMA), Louvain Drug Research Institute, Université Catholique de Louvain, Ave Mounier 73 − B1.73.08, B-1200 Brussels, Belgium. Tel: (+32) 2-7647364; E-mail: benedicte.jordan@uclouvain.be

Conflict of interest: none.

Supplementary material for this article can be found at www.redjournal.org.

Acknowledgment—The authors thank Chrystelle Po for development of the magnetic resonance postprocessing routine (R_1 biexponential deconvolution) and assistance with data analysis. TT Cao-Pham and F. Colliez are Televie Research Fellows, B.F. Jordan is Senior F.R.S./fNRS Research Associate.

Int J Radiation Oncol Biol Phys, Vol. 96, No. 1, pp. 149−160, 2016
0360-3016/$ - see front matter
http://dx.doi.org/10.1016/j.ijrobp.2016.04.029

oxygenation changes induced by carbogen. Yet, the R_1 parameters failed to predict the curability of a carbogen-sensitive model in a tumor control dose 50% assay, whereas R_2* was found to be correlated with RT outcome ($P<.05$).

was seen throughout the study between MR parameters and pO_2. Global and lipids R_1 were found to be correlated to pO_2 in the rhabdomyosarcoma model, whereas R_2* was found to be inversely correlated to pO_2 in the 9L-glioma model ($P=.05$ and .03). Carbogen increased the TCD50 of 9L-glioma but did not increase the GD of rhabdomyosarcoma. Only R_2* was predictive ($P<.05$) for the curability of 9L-glioma at 40 Gy, a dose that showed a difference in response to RT between carbogen and air-breathing groups. ^{18}F-FAZA positron emission tomography imaging has been shown to be a predictive marker under the same conditions.

Conclusion: This work illustrates the sensitivity of oxygen-sensitive R_1 and R_2* parameters to changes in tumor oxygenation. However, R_1 parameters showed limitations in terms of predicting the outcome of RT in the tumor models studied, whereas R_2* was found to be correlated with the outcome in the responsive model.

Introduction

Hypoxia is a common feature of solid tumors, which heralds a poor prognosis for cancer treatment, especially irradiation (1). Studies demonstrate that tumor hypoxia is highly individual dependent (2). Additionally, tumor hypoxia modification improves the outcome of cancer therapy and overall survival (2). So, there is a need for a reliable, robust, and easily conducted method for measuring tumor oxygenation that could allow radiotherapists to select an appropriate way to overcome hypoxia. Although many techniques have been investigated, there is still no available array of methods for routine practice (3, 4). Imaging allows repeatable measurements and appears to be an appropriate technique for assessing oxygenation because hypoxia extends spatially and temporally. Magnetic resonance imaging (MRI)-based endogen contrast techniques including R_1 and R_2* appear to be promising because MRI is noninvasive and nonionizing, and it does not require any injection of a reporter probe. R_1 is sensitive to dissolved molecular oxygen (5), whereas R_2* is sensitive to blood oxygenation, detecting changes in deoxyHb (6). Given that each technique assesses tumor hypoxia in different compartments, efforts are being made to combine R_1 and R_2* to better understand tissue oxygenation and to make use of the predictive value of these parameters for tumor response to radiation therapy (RT) (7, 8). Recently, O'Connor et al, as well as, Dewhirst and Birer (9, 10) validated oxygen-enhanced MRI (an R_1-based method) for quantifying the spatial variation of hypoxia with pimonidazole staining in 3 tumor lines with different hypoxic fractions. In 2013, we proposed an innovative noninvasive MRI R_1-based method for measuring tumor oxygenation. The method, with the acronym MOBILE (Mapping of Oxygen By Imaging relaxation Enhancement), is based on the assessment of lipids R_1 instead of global R_1 because oxygen is more soluble in lipids than in water (11). In this context, we expected that lipids R_1 should be more sensitive than global R_1 to the actual change in tumor oxygenation.

Our current work focuses on the assessment of R_2* and R_1 MR-derived parameters, including lipids R_1, water R_1, global R_1, and R_2*, as markers of tumor oxygenation and response to RT. Lipids R_1 and water R_1 were extracted using a biexponential deconvolution method (see Methods and Discussion sections). These MR biomarkers were compared with electron paramagnetic resonance (EPR) oximetry, which was used as a reference measurement of tumor pO_2 in vivo (12). MR acquisition was carried out under normoxic (air) and hyperoxic (carbogen, 95% O_2, 5% CO_2) conditions to evaluate the sensitivity of these MR parameters to changes in oxygenation. In addition, tumors were irradiated with or without hypoxia-driven intervention (carbogen) to evaluate the relation between RT outcome and MR parameters. In a previous study, it was determined by EPR oximetry and PET ^{18}F-FAZA that rhabdomyosarcoma and 9L-glioma had different hypoxic fractions and, importantly, that ^{18}F-FAZA was able to predict the outcome of RT in those models (13). The same protocol was used in this study to assess the predictivity of noninvasive MR parameters with regard to the outcome of RT.

Methods and Materials

Tumor models

Two tumor models were included in the study: rhabdomyosarcoma (n = 32) and 9L-glioma (n = 63). Fragments from a syngeneic rhabdomyosarcoma (1 mm^3) were grafted subcutaneously in 1 thigh of male adult WAG/Rij rats, according to a model developed by the Laboratory of Experimental Radiobiology, Katholieke Universiteit Leuven, Belgium. 9L-glioma cells were grown in Roswell Park Memorial Institute (RPMI) medium supplemented with 10% fetal calf serum (heat inactivated), 1% of a mixture of antibiotics (penicillin 100 UI/mL, streptomycin 0.1 mg/mL), 1% nonessential amino acids, and 1% sodium pyruvate. Cells were maintained in a balanced wet atmosphere (37°C and CO_2 5%). To establish 9L-glioma tumors in vivo, male adult Fisher F344 rats were inoculated subcutaneously in their thighs with 5.10^6 cells. Tumor implantations were performed with the rats under general

anesthesia with intraperitoneal injection of ketamine and xylazine (80 and 10 mg/kg, respectively) on rats weighing between 200 and 250 g. The animals were introduced into the study when the tumors reached the size of 15 to 20 mm.

Experimental design

The study was approved by the local ethics committee. Studies were undertaken in accordance with the national and local regulations of the ethical committee (agreement number UCL/2010/MD/001).

Rhabdomyosarcoma

Four cohorts were involved. An experiment course of 3 days was designed for the first and second cohorts (Fig. E4A; available online at www.redjournal.org). For the first 2 days, animals of these 2 cohorts underwent the same procedure. Rats were anesthetized with isoflurane 1.5% for all interventions. Gas delivery (medical air or carbogen mixed with isoflurane) was continuous at 2 L/min through a nosepiece. On day 1, animals were subjected to MRI studies for R_1 and R_2* measurements. On day 2, tumor pO_2 was measured by EPR oximetry. All MR measurements were conducted under baseline and hyperoxic condition, which was obtained after 30 minutes of carbogen breathing. On day 3, rats were divided randomly into 2 subgroups for irradiation at 20 Gy under either air or carbogen breathing for growth delay (GD) assay (13). A third nonirradiated non-MRI control cohort was included. The fourth cohort was assigned to verify the repetition of tumor oxygenation over a period of 48 hours (Table E1; available online at www.redjournal.org). The details of the experimental design and the number of animals used in each cohort are presented, respectively, in Figures E4A and E4B (available online at www.redjournal.org).

At least twice a week, tumor size was assessed by a caliper and measured as the average of the longest and the shortest perpendicular diameters until the tumors reached 30 mm. The GD was calculated as the time after irradiation required for a tumor to grow to 1.5 times D_0, the tumor size at the time of treatment or at the beginning of the follow-up period (for control animals).

9L-glioma

There were 2 experimental series. For the first series, animals were randomly divided in 2 groups for baseline and carbogen challenge. Tumor was subjected to R_1 and R_2* acquisition and was then irradiated under the same breathing condition. In each group of breathing conditions, animals were randomly allocated in 5 subgroups, with the irradiation dose ranging from 10 to 60 Gy. For the second series, the same experiment as in the first and second cohorts of rhabdomyosarcoma was applied (Fig. E4A; available online at www.redjournal.org). Animals were irradiated at 40 Gy on the third day.

Details on numbers of animals can be found in Table E2 (available online at www.redjournal.org). Of note in the group irradiated at 40 Gy, data included all tumors of the second series, and those who received 40 Gy of RT in the first series.

Tumors were followed up until their diameters reached 30 mm. Animals were considered to be cured because there was no tumor regrowth at day 120 after irradiation. Responses to RT of 2 series were summed on tumor cure assay, which is known to be the most relevant assay for clinical translation.

MR measurements

Magnetic resonance imaging was performed on a 11.7-Tesla, 16-cm inner diameter bore system (Bruker, Biospec) with a 7-cm birdcage coil for signal emission and a surface coil for signal reception. A warm water blanket was used to maintain the animal's temperature at 37°C, and the temperature was monitored with an MR-compatible rectal probe.

A multislice Rapid Acquisition with Relaxation Enhancement (RARE) sequence was first used to determine the most representative tumor slice for further measurement, with the following parameters: echo time (TE)/Repetition time (TR)/RARE-factor/field of view (FOV)/matrix size/slice thickness = 10.66 ms/2500 ms/6/35 × 35 mm/256 × 256/1 mm. The segmented IR-FISP sequence (SSFP-FID mode) was used for R_1 acquisition with the following parameters: TR/TE/FA/BW/FOV/matrix size/slice thickness = 4 ms/1.35 ms/10°/100 kHz/55 × 30 mm/100 × 85/1 mm, 4 segments, 100 TI from 13 ms to 8329 ms every 84 ms, and a total acquisition time of 20 minutes. Multi-Gradient Echo R_2* images were acquired at TR/FA/slice thickness = 3000 ms/15°/1 mm with a FOV of 35 × 35 mm on a 256 × 256 matrix, 12 echoes from 3.5 ms to 58.5 ms every 5 ms. The total acquisition time was 9 minutes 36 seconds.

The EPR spectroscopy permitted a direct measurement of tumor oxygenation through the conversion of EPR linewidth to pO_2 by using a calibration curve (14). The method of EPR data acquisition has been described elsewhere (12). Briefly, charcoal wood powder (CX0670-1, EM Science, Gibbstown, NJ) was used as an oxygen-sensitive sensor. About 200 μL charcoal suspension (100 mg/mL) was introduced within tumor at a depth of 3 to 6 mm using a 23-gauge needle on day 1, after MRI acquisitions. The EPR experiments were performed 24 hours after probe implantation by using an L-band EPR spectrometer (Magnettech, Berlin, Germany) equipped with a low-frequency microwave bridge operating at 1.2 GHz and a loop-gap resonator. For that purpose, animals were anesthetized for EPR measurement. and tumors were placed at the center of the loop-gap resonator, whose sensitivity extends to 1 cm around the loop. The modulation frequency was 100 kHz,

and the amplitude modulation was less than one-third of the peak-to-peak linewidth to avoid peak distortion. The linewidth of the first derivative EPR spectrum that was the average of 5 scan accumulations was then converted to pO_2 using a calibration curve. After the pO_2 value was recorded under normoxic conditions, the rats were allowed to inhale carbogen for 30 minutes, and the acquisition was then repeated to obtain the value of pO_2 with the rats under hyperoxic conditions.

Irradiation

Tumors received a single dose of irradiation delivered by a ^{137}Cs irradiator IBL-637 (Oris, France). The dose rate was equal to 1 Gy/min. Animals were anesthetized with isoflurane 1.5% and were placed on a lead brick 3-mm thick to protect from whole-body irradiation while the tumors were exposed through a hole 25 mm in diameter. Tumors were turned midway through the exposure time to ensure homogeneity of dose distribution. For the carbogen group, the animals were allowed to inhale carbogen at 2 L/min for 5 minutes before and during irradiation (15).

Data analysis and statistics

Data analysis was performed on an in-house program developed under ImageJ and MATLAB. R_1s and R_2* maps were calculated with an MRI analysis calculator plug-in in ImageJ software. This MRI analysis method is adapted from the original plugin created by Karl Schmidt (http://rsb.info.nih.gov/ij/). The method use a curve fitting method based on the Simplex method described Caceci and Cacheris (16). Lipids R_1 and water R_1 were extracted from the global R_1 map by a biexponential deconvolution method. Regions of interest (ROIs) were drawn manually around the tumor on the selected anatomic slice and were transferred to all R_2* and R_1s maps of the same slice. The subtraction of 2 maps air and carbogen is done pixels par pixels, resulting in maps of delta.

Normality of the data distribution was checked before selection of the appropriate statistics using a normal quantile plot. Statistical significance of changes between MR parameters before and after carbogen challenge was assessed with the Student paired *t* test (Figs. 1 and 2). Values were expressed as mean ± standard equivalent of the mean or as relative variations.

The linear association between MR parameters and pO_2 measured using EPR (Fig. 3) was tested by correlation analysis. Pearson *R* coefficient was considered statistically significant for $P<.05$.

Response of the rhabdomyosarcoma to 20-Gy irradiation (GD curves, Fig. 4A) was analyzed with a linear mixed model. Fixed effects included in the model were the group, the time, and the interaction between the group and the time. Random effects included were a random intercept and a random slope. Linear relation between the GD and MR

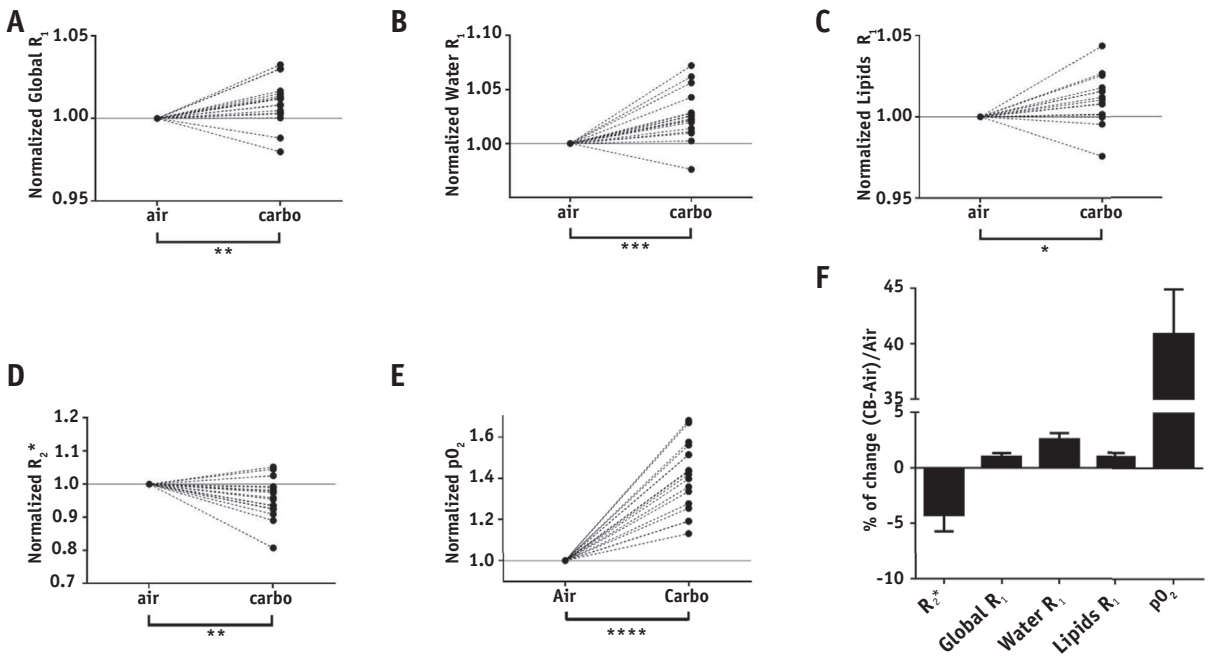

Fig. 1. Changes in magnetic resonance (MR) parameters in second series of 9L-glioma (n = 17), baseline and hyperoxic conditions. (A-E) Individual normalized changes after carbogen challenge. (F) Mean relative changes ± standard equivalent of the mean (%). All MR parameters could track the change in tumor oxygenation induced by carbogen. *Abbreviation:* Carbo = carbogen.

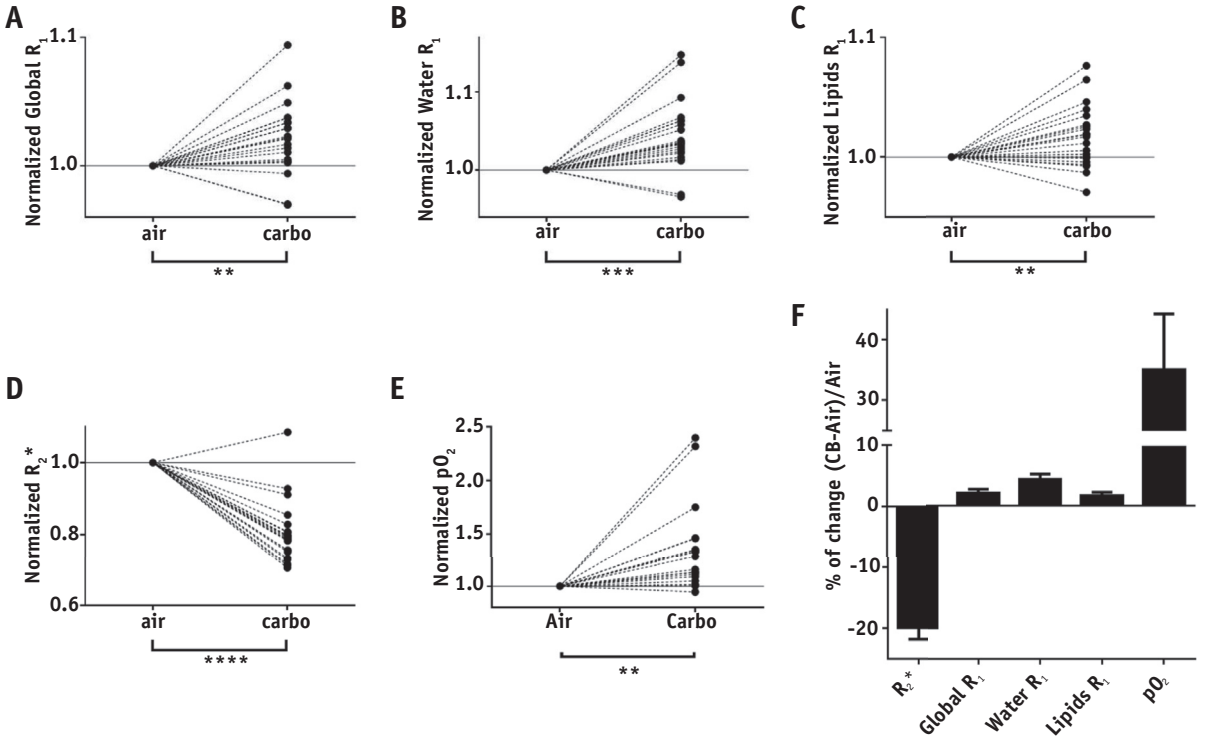

Fig. 2. Changes of magnetic resonance (MR) parameters in rhabdomyosarcoma (n = 19-22) of baseline and hyperoxic condition. (A-E) Individual normalized changes after carbogen challenge. (F) Mean relative changes ± standard equivalent of the mean (%). All MR parameters could track the change in tumor oxygenation induced by carbogen. *Abbreviation:* Carbo = carbogen.

parameters was tested in the rhabdomyosarcoma model by correlation tests (Fig. 4B-F).

With respect to the TCD50 assay in the 9L-glioma model, the predictive value of pretreatment (air vs carbogen) MRI (R_2*, global R_1, water R_1, lipids R_1) parameters on RT (40 Gy) treatment outcome was tested by logistic regression. For MRI parameters, multicollinearity was first checked. Based on the correlation matrix, global R_1 and lipids R_1 were found to be highly correlated. Two different models were built, 1 including global R_1 and 1 including lipids R_1 in the logistic model. The models were validated with the likelihood-ratio χ^2 value (model 1, $P = .0036$; model 2, $P = .0032$) (Table 1).

In the 9L-glioma group irradiated at 40 Gy, the difference of MRI parameters between cured and uncured animals was assessed with the Wilcoxon rank-sum scores because of a nonnormal distribution of the data.

Optimal sample size was computed by use of nQuery 2.0 with an α of 0.05 and a power of 0.8.

Statistical analyses were performed with the GraphPad (Prism) program, JMP Pro 12 (SAS Institute, Cary, NC), and SAS 9.4 for the mixed model.

Results

Representative parametric maps of spatial distribution of carbogen-induced ΔR_2*, water ΔR_1, lipids ΔR_1, global ΔR_1, and EPR spectra taken under air and carbogen breathing conditions in rhabdomyosarcoma and 9L-glioma are presented in Figure E1 (available online at www.redjournal.org). All MRI maps show heterogeneity within tumors in response to carbogen, with a mixture of pixels sensitive to and refractory to carbogen challenge, similar to that in the data shown in a recent study assessing R_1 in response to an oxygen challenge (17). In both models, carbogen generated an increment of pO_2 that broadened the linewidths of EPR spectra.

Figures 1 and 2 present precarbogen and postcarbogen challenge MR data for 9L-glioma and for rhabdomyosarcoma, respectively. The purpose was to study the ability of the breathing treatment to induce changes in oxygenation and to assess the values of the MR parameters reflecting this change. Information on the change in MR intrinsic values for 9L-glioma and rhabdomyosarcoma can be found in Figures E2 and E3 (available online at www.redjournal.org).

A rise in pO_2 resulted in a larger R_1. Global R_1 increased after carbogen from 2.23 ± 0.04 s^{-1} to 2.25 ± 0.04 s^{-1} in 9L-glioma (n = 17, $P = .008$) (Fig. 1A) and from 2.14 ± 0.02 s^{-1} to 2.19 ± 0.02 s^{-1} in rhabdomyosarcoma (n = 22, $P = .002$) (Fig. 2A). The response of global R_1 to carbogen breathing was quite similar in both models: 2 9L-glioma tumors (12%) and 3 rhabdomyosarcoma tumors (14%) had a negative global ΔR_1 (Figs. 1A and 2A). Water R_1 and lipids R_1 demonstrated the same trend. In response

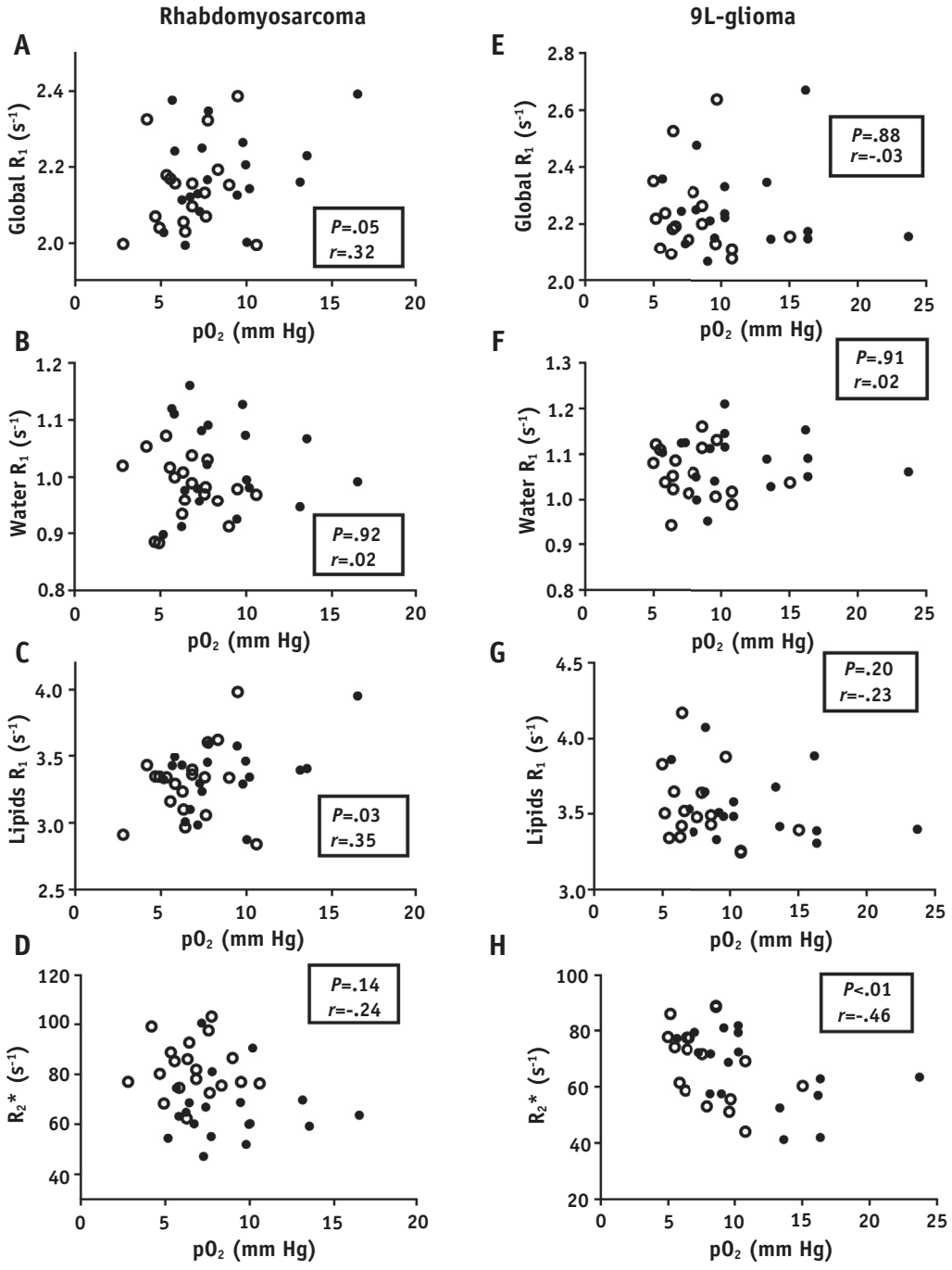

Fig. 3. Correlation between different magnetic resonance parameters with pO_2 assessed by electron paramagnetic resonance oximetry. Left (A-D), Rhabdomyosarcoma. Right (E-H), 9L-glioma. Each point was representative for an individual tumor subjected either to room air (open symbol) or to carbogen (filled symbol).

to carbogen breathing, the water R_1 increased from 1.06 ± 0.01 s^{-1} to 1.09 ± 0.02 s^{-1} ($P = .0003$) (Fig. 1B) and from 0.98 ± 0.01 s^{-1} to 1.03 ± 0.02 s^{-1} ($P = .0002$) (Fig. 2B) in 9L-glioma and rhabdomyosarcoma, respectively. We observed an even transition of this parameter generated by carbogen, whereas 6% of the 9L-glioma (1 tumor) and 9% of the rhabdomyosarcoma (2 tumors) did not respond to the challenge (Figs. 1B and 2B). The change was less pronounced for lipids R_1. Lipids R_1 was, respectively, 3.54 ± 0.06 s^{-1} (baseline) and 3.56 ± 0.05 s^{-1} (hyperoxic) ($P = .0196$) in 9L-glioma (Fig. 1C) and 3.30 ± 0.05 s^{-1} (baseline), 3.35 ± 0.05 s^{-1} (hyperoxic) ($P = .0051$) in rhabdomyosarcoma (Fig. 2C). Eighteen percent of the 9L-glioma (3 tumors) and 27% of the rhabdomyosarcoma (6 tumors) did not respond to carbogen breathing (Figs. 1C and 2C).

When blood oxygenation went up, dHb decreased as an effect of the increase of HbO_2; this led to a decrease in R_2*.

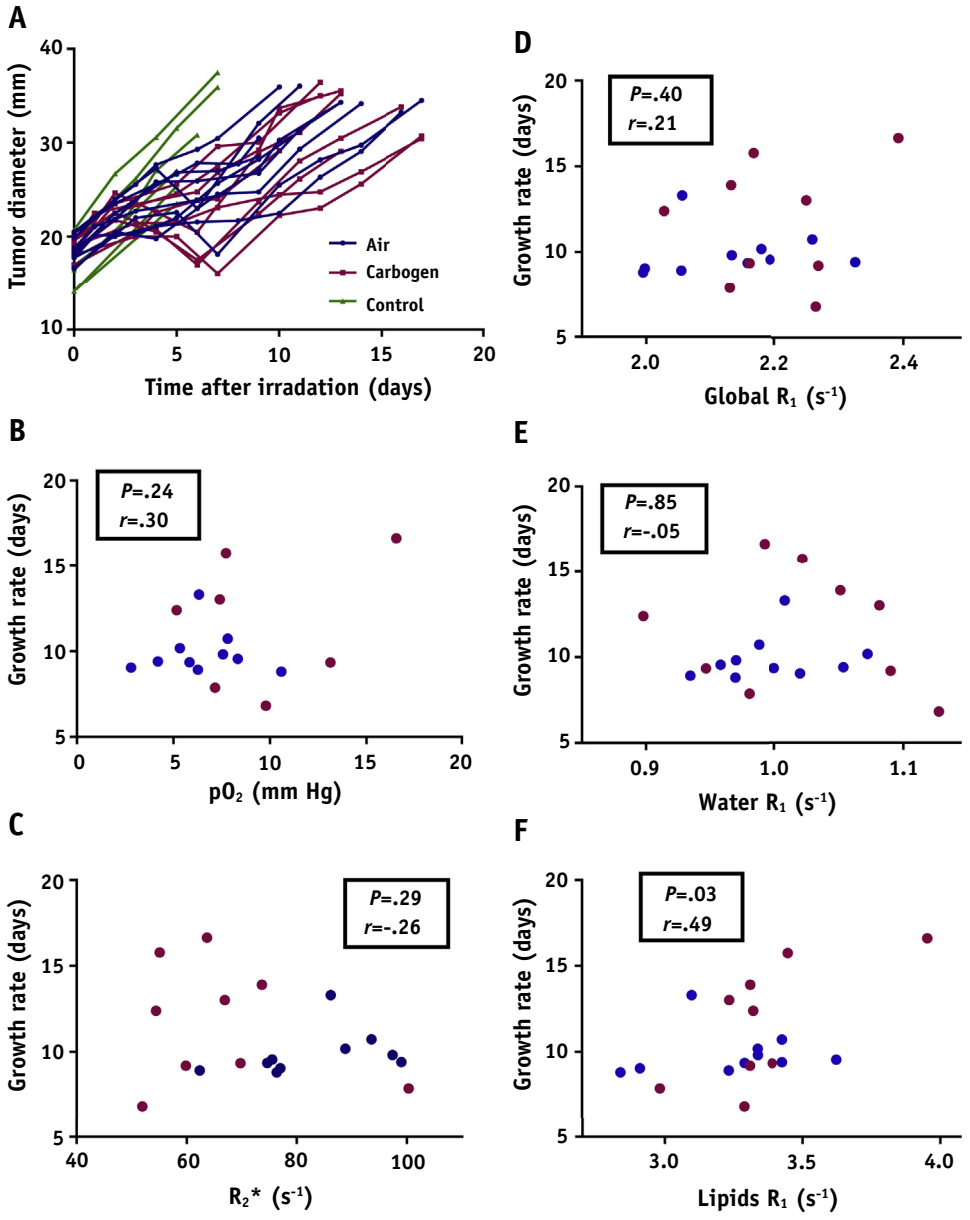

Fig. 4. (A) Response of rhabdomyosarcoma to irradiation of 20 Gy (control n = 6, baseline n = 10, carbogen n = 9). (B-F) Relationship between magnetic resonance parameters and growth delay in rhabdomyosarcoma (n = 19, except B n = 17). Each point represents a tumor irradiated under baseline (blue symbols) or carbogen breathing condition (red symbols). Note, we expected a negative slope for R_2* and pO_2 correlation and a positive slope for R_1 correlation.

Carbogen reduced R_2* in 9L-glioma (n = 17) from 68.72 ± 3.30 s^{-1} to 65.73 ± 3.14 s^{-1} ($P = .01$) (Fig. 1D) and from 82.79 ± 2.18 s^{-1} to 66.44 ± 2.63 s^{-1} ($P < .0001$) (Fig. 2D) in rhabdomyosarcoma (n = 22). The R_2* alteration showed that both models were responsive to the carbogen challenge (Figs. 1F and 2F). Three glioma did not respond to carbogen in terms of R_2*, versus 1 rhabdomyosarcoma. Interestingly, the tumors that showed a lack of response in terms of R_1 were different from those that showed a lack of response in terms of R_2*.

These MR parameters were compared with the pO_2 obtained by EPR. Carbogen breathing increased pO_2 from 8.0 ± 0.6 mm Hg to 11.4 ± 1.1 mm Hg in 9L-glioma (n = 17) ($P < .0001$) (Fig. 1E) and from 6.7 ± 0.4 mm Hg to 8.7 ± 0.7 mm Hg in rhabdomyosarcoma (n = 19) ($P = .0008$) (Fig. 2E). Whereas the pO_2 of all the 9L-glioma increased on hyperoxic challenge (Fig. 1E), the pO_2 of 1 rhabdomyosarcoma decreased (Fig. 2E). Note that only the pO_2 in 9L-glioma increased beyond 10 mm Hg. Interestingly, changes in R_1s and R_2* induced by a rise in pO_2, observed here by EPR oximetry, matched those seen with use of the OxyLite system (fluorescence-quenching fiberoptic-based method) by O'Connor et al (10), showing that changes in MRI parameters are reproducible across different tumor models and laboratories.

Table 1 Logistic regression and odds ratio

Variable	Coefficient (β)	Standard error	*P* value	Odds ratio	95% Confidence interval
Intercept	43	29	.14	-	-
Air/carbogen	−2.8	1.27	.0006	270	6.5-5.17 10^{5}
R_2* (s^{-1})	0.26	0.14	.0094	1.29	1.05-1.92
Lipids R_1 (s^{-1})	−9.8	5.9	.021	5.2 10^{-5}	3.8 10^{-12} to 3 10^{-1}
Water R_1 (s^{-1})	−21.6	19.3	.205	4.3 10^{-10}	2.9 10^{-33} to 4.4 10^{4}
Intercept	34	29	.24	-	-
Air/carbogen	−2.34	1.11	.002	106	4-6.6 10^{4}
R_2* (s^{-1})	0.22	0.12	.012	1.25	1.04-1.76
Global R_1 (s^{-1})	−15.7	10.5	.019	1.5 10^{-7}	2.6 10^{-21} to 0.14
Water R_1 (s^{-1})	−10.8	16.2	.48	2.0 10^{-5}	8.33 10^{-23} to 1.34 10^{8}

Above, model includes lipids R_1 as explicative variable but not global R_1. Below, model includes global R_1 but not lipids R_1.

To study the quantitative aspect of MRI biomarkers, we correlated individual MRI parameters and their corresponding pO_2 under distinct breathing conditions (Fig. 3). As discussed above, an increase in pO_2 resulted in a decrease in R_2* and an increase in R_1. Thus, theoretically, we expect a negative slope in pO_2-R_2* correlation and a positive slope in pO_2-R_1 correlation. The correlations were found to be significant in global R_1-pO_2 and in lipids R_1-pO_2 for rhabdomyosarcoma ($P = .05$ and .03, respectively) (Figs. 3A and 3C) and in R_2*-pO_2 for 9L-glioma ($P < .01$) (Fig. 3H).

Figure 4 presents the GD assay (Fig. 4A) and the correlations between RT responses with different MR parameters in rhabdomyosarcoma (Fig. 4B-F). The mixed model analysis did not show any difference between groups, meaning that carbogen was not able to significantly radiosensitize this tumor model, and did show an influence of time. As R_1 becomes larger, tumor oxygenation is higher; thus, a longer GD is expected. In that case, the slopes correlating R_1 and GD should theoretically increase (Fig. 4D-F). For R_2* the slope should theoretically decrease because a shorter R_2* corresponds to a higher oxygen level (Fig. 4C). A similar trend should be observed for correlation with pO_2 (Fig. 4B). Here, only the correlation between lipids R_1 and GD was found to be significant ($P = .03$, $R = .49$) (Fig. 4F). Note that actual pO_2 values also did not correlate with GD and that this might be due, in part, by the lack of individuals with high pO_2 values.

It should be noted that for rhabdomyosarcoma, 22 rats underwent MRI acquisition. However, the EPR signals of 3 rats were not exploitable. These 22 animals were then irradiated under either air or carbogen breathing; 3 died before the TGD experiment ended. Briefly, 17 had complete MRI, TGD, and EPR information; 2 had MRI and TGD information; 2 had MRI and EPR information; and 1 had only MRI information; this explains the discrepancy in the number of results in this model.

A TCD50 assay was performed on 9L-glioma. Figure 5 shows the radiation dose-response curves for tumor curability 120 days after irradiation. Carbogen decreased the TCD50 from 41.6 Gy in the group irradiated under air breathing conditions (95% confidence interval, 38.5-44.6 Gy) to 32.2 Gy in the group irradiated under carbogen breathing conditions (95% confidence interval, 31.8-32.6 Gy). The dose-modifying factor DMF50 was 1.29, obtained by dividing the TCD50 of the group irradiated under carbogen breathing by that of the radiation-alone group. Inasmuch as the DMF value was greater than 1, we conclude that carbogen enhanced the radioresponse of 9L-glioma tumor.

To evaluate the predictivity of MR biomarkers in RT (40 Gy) outcome, we performed a logistic regression (Table 1).

The first logistic analysis (using lipids R_1, water R_1, R_2*, carbogen/air) showed a significant predictive value for the carbogen pretreatment ($P = .0006$) and for R_2* ($P = .009$) and lipids R_1 ($P = .02$). Water R_1 was not significant ($P = .20$). In other terms, the carbogen group was 270 times more likely in terms of odds to have a positive RT outcome than was the air-treated group (odds ratio [OR] 270, CI 6-517,155). With regard to MRI parameters, tumors with a lower R_2* were 29% more likely in terms of odds to have a positive RT outcome (OR per unit 1.29; CI 1.05-1.92). The odds ratio for lipids R_1 was 5.25 10^{-5} (CI 3.87 10^{-12}-0.30). The odds probability ratio over the entire range was 830,137 for R_2* compared with 0.000128 for lipids R_1. The predictive value of R_2* is consequently likely to be of greater interest than that of lipids R_1.

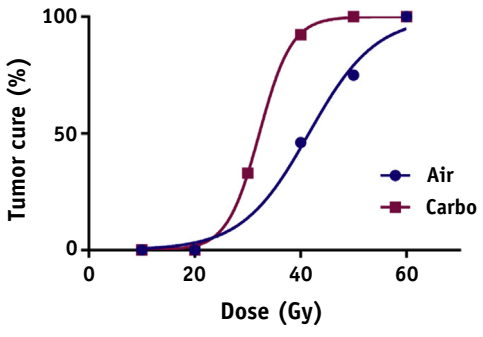

Fig. 5. Tumor cure assay on 9L-glioma 120 days after irradiation. *Abbreviation:* Carbo = carbogen.

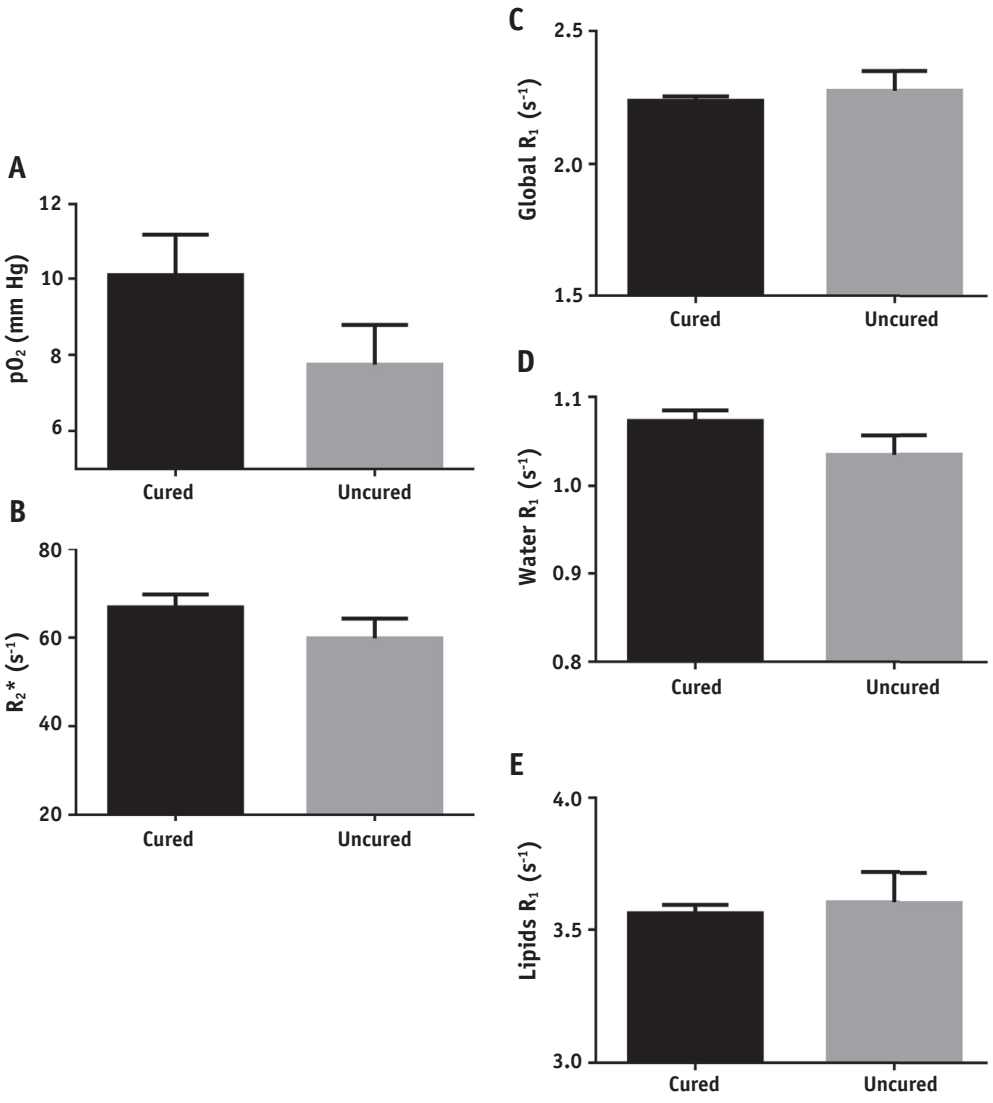

Fig. 6. Comparison of intrinsic magnetic resonance parameters between cured (n = 18) and uncured group (n = 8) of 9L-glioma tumors irradiated at 40 Gy (n = 26), (except A, cured n = 12, uncured n = 5). No magnetic resonance parameter was predictive for the curability of the 9L-glioma model. A: pO_2 (mmHg) assessed using EPR oximetry; B: R_2* MR parameter; C: Global R_1 MR parameter; D: Water R_1 MR parameter; E: Lipids R_1 MR parameter.

The second logistic model (using global R_1 instead of lipids R_1) showed similar results, confirming the strong correlation between global R_1 and lipids R_1 (OR carbogen/air 106, CI 4-66.448; OR R_2* 1.25, CI 1.04-1.76; global R_1 1.5 10^{-7}, CI 2.6 10^{-21}-0.14). The predictive value of R_2* is consequently likely to be of greater interest than that of global R_1.

We also compared the MR intrinsic values of cured (n = 18) and uncured (n = 8) groups irradiated at 40 Gy (Fig. 6). The data in Figure 6A refer to tumors in the second series which underwent the EPR measurement (cured n = 12, uncured n = 5). None of the parameters showed a significant difference between the cured and uncured groups, although the actual pO_2 values assessed by EPR oximetry do show that the cured group presented pO_2 values around 10 mm Hg, which is the theoretical radiosensitivity threshold, unlike the uncured group, which presented values around 8 mm Hg and therefore below this threshold. It should be noted that the statistical test used was nonparametric, inasmuch as the distribution was non-normal. Although robust, this test requires a large sample size to demonstrate a difference. In this particular case, the required size sample would be 31 animals per group at a risk level α of 0.05 and a power of 0.8.

Discussion

This work had 2 goals: (*1*) to assess the sensitivity of oxygen-sensitive MR parameters to changes in tumor oxygenation, including lipids R_1, water R_1, global R_1, and R_2*, in comparison with pO_2 assessed by EPR oximetry;

and (*2*) to correlate the tumor response to irradiation with these MR parameters to assess the relevance of each parameter as a potential predictive marker of the outcome of RT.

The modulation of tumor oxygenation was achieved by carbogen (5% CO_2 95% O_2) breathing. Because many factors can influence the oxygen modulation capacity of carbogen, tumors do not respond to this gas systematically. Thus, we selected tumor models that have previously been described to respond to carbogen (13). The purposes of using carbogen were: (*1*) to improve the understanding of different MR oxygen-sensitive parameters; and (*2*) to interpret these parameters in the context of outcome of RT.

For R_1 parameters, we observed that carbogen generated significant increases in all R_1 MR-derived parameters (global R_1, water R_1, lipids R_1) corresponding to the increases in pO_2 assessed by EPR oximetry (Figs. 1 and 2). Nevertheless, when R_1 parameters were compared, the response of lipids R_1 was less pronounced than that of global or water R_1, contrary to our assumption. The lipids R_1 values obtained in this work seemed less sensitive than those presented in a previous work (11, 18). The discrepancy could be due to different imaging acquisition sequences. The earlier work used 2 distinct sequences for global R_1 and lipids R_1. However, this sequence worked only on tumor models with a high amount of lipids (ie, mammary tumor models). In this study, we used 2 tumor models with a lower lipid content, and therefore we needed to adapt the type of acquisition (1 acquisition for global R_1, biexponential deconvolution of the signal to extract fast and slow components). The fast and slow components are attributed to lipids and water relaxation (19), but we cannot exclude a contribution to the fast component from water linked to macromolecules. In fact, water exists both in blood and tissue, and water R_1 represents the variation of oxygen in both compartments. However, water may be present in tissue under multiple states, ranging from unbound to partially structured or fully bound to macromolecules. Although these bound water protons are in the minority, they do have a significant relaxation effect on R_1. Water that forms a hydration layer around macromolecules has restricted motion. This leads to an increase in R_1 because those water protons are involved in interactions near the Larmor frequency (20, 21). The membrane phospholipids of blood cells barely contribute to the lipids R_1 signal because the substance participates only in oxygen exchange. Consequently, lipids R_1 can probably account only for lipids in tissue. Hence, the results obtained could be explained by the fact that water R_1 reflects the oxygen in blood and tissue, and lipids R_1 focuses mostly on oxygen in tissues. Inasmuch as global R_1 takes account of both fast and slow relaxation rates, its response is intermediate. In fact, 2 approaches could be considered to modulate tumor oxygenation: modification of oxygen consumption or of oxygen supply. Carbogen could increase the oxygen supply through arterial blood saturation, but it does not necessarily produce the same effect on tumor oxygenation. Hence, we assumed that the sensitivity of lipids R_1 depends on the type of modulation of tumor oxygenation. For a better understanding of lipids R_1 behavior, additional studies should be performed with pharmacologic agents able to modulate the oxygen consumption of tumor cells.

With regard to the quantitative aspect of R_1s, correlations of global R_1 and lipids R_1 were significant in the rhabdomyosarcoma model, which is less responsive to carbogen (Figs. 3A and 3C) but not in the more carbogen-responsive 9L-glioma model, where R_2^* was found to be significant (Fig. 3H). In healthy mouse brain, Beeman et al (22) showed that R_1 was linearly dependent on pO_2 assessed by optical probe, using 3 breathing conditions: hypoxic gas, 100% O_2, and carbogen. In addition, the ΔR_1 of hypoxic gas and carbogen could discriminate between normal brain, radiation-induced lesions, and tumor lesions. In a report by O'Connor et al (23), a different approach to analyzing R_1 maps was investigated. Comparing R_1 maps for air breathing and 100% O_2 breathing, they hypothesized that tumor fractions that had R_1 refractory to oxygen challenge ($\Delta R_1 < 0$) would be a key biomarker of hypoxia, not ΔR_1 or ΔR_2^*. The work provided evidence that the "oxy refractory fraction" along with DCE MRI was able to determine the hypoxia fraction in different models. Furthermore, this parameter was also sensitive to dynamic changes in tumor oxygenation. That study work also emphasizes the potential valued of analyzing intratumor heterogeneity (23).

For R_2^*, the paramagnetic dHb generates a field gradient that causes an increase in R_2^* not only in the water of blood plasma but also in neighboring tissues. Consequently, R_2^* drops if the dHb concentration per unit of tissue volume decreases, either by a reduction of dHb concentration in the blood or by a decrease in blood volume. In this context, carbogen generated a decrease in R_2^* in both tumor models. These changes result not only from the decrease of dHb in the blood resulting from the binding of oxygen-hemoglobin but also from the contribution of other factors. Some possible changes induced by carbogen that influence the R_2^* signal are modification of tumor blood flow, pH, response of tumor vessels, or tumor blood volume. Although these effects are minor and are normally outweighed by the decrease in dHb while breathing carbogen, they still contribute to the change in R_2^* image intensity. Briefly, R_2^* represents more than just vessel oxygenation, and ΔR_2^* induced by carbogen reflects both the hemodynamic and vasoactive response of the tumor to CO_2 in combination with the real change in blood oxygenation. In this context, R_2^* was found to be inversely correlated with pO_2 in 9L-glioma ($P < .01$) (Fig. 3H). In addition, ΔR_2^* in rhabdomyosarcoma ($16.34 \pm 1.59\ s^{-1}$) was larger than in 9L-glioma ($2.98 \pm 0.97\ s^{-1}$), whereas ΔpO_2 in 9L-glioma (3.5 ± 0.5 mm Hg) was more intense than in rhabdomyosarcoma (2.1 ± 0.5 mm Hg). Although the R_2^* response is individual dependent, it is interesting to note that R_2^* is more sensitive when the basal oxygenation level is lower (24) (the baseline pO_2 of rhabdomyosarcoma

and 9L-glioma are 6.7 ± 0.4 mm Hg and 8.0 ± 0.6 mm Hg, respectively).

Obviously, understanding the mechanisms behind the responses of MR parameters to the changes in tumor oxygenation is helpful. But above all, the more fundamental need in clinical practice is to address the question of whether these MR methods can predict the outcome of radiation therapy. In both models, carbogen induced significant changes in all MRI parameters, reflecting an increase in tumor oxygenation. These modifications were confirmed by pO_2 assessed by EPR. However, irradiation under carbogen breathing conditions significantly increased the survival of 9L-glioma but not of rhabdomyosarcoma. This established a paradigmatic situation with 1 responsive and 1 unresponsive model. With respect to the distinct radiosensitive properties of the 2 tumor models, we conducted a GD assay on the rhabdomyosarcoma model and a more clinically relevant TCD50 assay on the 9L-glioma model.

The GD was performed at 20 Gy. Indeed, in a preceding study (13), the RT dose escalation from 15 Gy to 20 Gy significantly increased the response to irradiation in rhabdomyosarcoma. Yet, there was no benefit of carbogen on RT response between animals irradiated under air versus carbogen breathing conditions. Thus, we decided to remain at this dose rate to further correlate the GD and MR parameters. Lipids R_1 was correlated with the GD in rhabdomyosarcoma (Fig. 4F). A lack of correlation between GD and pO_2 was observed, which could be due to the lack of radiosensitive individuals (pO_2 >10 mm Hg) in this correlation (Fig. 4B).

In 9L-glioma, the more clinically relevant TCD50 assay confirmed the radiosensitizing properties of carbogen in this model. We selected the dose of 40 Gy to assess the predictivity of intrinsic MRI parameters because we observed a clear difference in response to irradiation between the 2 groups (carbogen vs air breathing). R_2* alone was likely to be predictive for the curability of 9L-glioma in this assay, whereas all R_1-related parameters failed to predict RT outcome.

Briefly, the R_1s and R_2* could tackle the individual change in tumor oxygenation induced by carbogen breathing. Yet, only R_2* was likely to predict the outcome of RT in 9L-glioma (tumors with a lower R_2* were 29% more likely to have a positive RT outcome), whereas ^{18}F-FAZA was shown earlier to be able to robustly predict the outcome of RT with a similar protocol. A possible explanation is the high heterogeneity between and within individuals (Fig. E1; available online at www.redjournal.org) and the influence of bound water on the long R_1 component. Nonetheless, the combination of R_2* and R_1 parameters should be further characterized in tumor models that are still more responsive to carbogen breathing and with other modulators of tumor oxygenation, including inhibitors of oxygen consumption. Alternative methods to extract R_1 of lipids should also be considered.

With respect to the translational aspect of the techniques, R_2* and R_1 have been applied to multiple patient studies at 1.5 T for R_2* (25, 26) and for R_1 (5), and 3T for R_2* (27) and for R_1 (28), which shows that these techniques can translate across multiple body sites and tumor types. A higher sensitivity of R_1 and a lower sensitivity of R_2* can be expected at lower magnetic fields than the 11.7 T used in the current study, yet more adapted to small animal studies.

In conclusion, this work illustrates the sensitivity of R_1 oxygen-sensitive MR parameters to changes in tumor oxygenation but shows their limitations in terms of predicting the outcome of RT in the tumor models under study, whereas R_2* was found to be partially correlated with the outcome in the carbogen responsive model. In line with the recent comment by Dewhirst and Birer (9) on oxygen-enhanced MRI, additional studies are needed to further validate MRI parameters for future patient stratification for hypoxia modification.

References

1. Harris AL. Hypoxia: A key regulatory factor in tumour growth. *Nat Rev Cancer* 2002;2:38-47.
2. Overgaard J. Hypoxic radiosensitization: Adored and ignored. *J Clin Oncol* 2007;25:4066-4074.
3. Vikram DS, Zweier JL, Kuppusamy P. Methods for noninvasive imaging of tissue hypoxia. *Antioxid Redox Signal* 2007;9:1745-1756.
4. Tatum JL. Hypoxia: Importance in tumor biology, noninvasive measurement by imaging, and value of its measurement in the management of cancer therapy. *Int J Radiat Biol* 2006;82:699-757.
5. O'Connor JP, Naish JH, Parker GJ, et al. Preliminary study of oxygen-enhanced longitudinal relaxation in MRI: A potential novel biomarker of oxygenation changes in solid tumors. *Int J Radiat Oncol Biol Phys* 2009;75:1209-1215.
6. Robinson SP, Rijken PF, Howe FA, et al. Tumor vascular architecture and function evaluated by non-invasive susceptibility MRI methods and immunohistochemistry. *J Magn Reson Imaging* 2003;17:445-454.
7. Burrell JS, Walker-Samuel S, Baker LC, et al. Exploring ΔR_2* and ΔR_1 as imaging biomarkers of tumor oxygenation. *J Magn Reson Imaging* 2013;38:429-434.
8. Hallac RR, Zhou H, Pidikiti R, et al. Correlations of noninvasive BOLD and TOLD MRI with pO_2 and relevance to tumor radiation response. *Magn Reson Med* 2014;71:1863-1873.
9. Dewhirst MW, Birer SR. Oxygen-enhanced MRI is a major advance in tumor hypoxia imaging. *Cancer Res* 2016;76:769-772.
10. O'Connor JP, Boult JK, Jamin Y, et al. Oxygen-enhanced MRI accurately identifies, quantifies, and maps tumor hypoxia in preclinical cancer models. *Cancer Res* 2016;76:787-795.
11. Jordan BF, Magat J, Colliez F, et al. Mapping of oxygen by imaging lipids relaxation enhancement: A potential sensitive endogenous MRI contrast to map variations in tissue oxygenation. *Magn Reson Med* 2013;70:732-744.
12. Gallez B, Baudelet C, Jordan BF. Assessment of tumor oxygenation by electron paramagnetic resonance: Principles and applications. *NMR Biomed* 2004;17:240-262.
13. Tran LB, Bol A, Labar D, et al. Potential role of hypoxia imaging using ^{18}F-FAZA PET to guide hypoxia-driven interventions (carbogen breathing or dose escalation) in radiation therapy. *Radiother Oncol* 2014;113:204-209.
14. Jordan BF, Baudelet C, Gallez B. Carbon-centered radicals as oxygen sensors for in vivo electron paramagnetic resonance: Screening for an optimal probe among commercially available charcoals. *MAGMA* 1998;7:121-129.

15. Tran LB, Bol A, Labar D, et al. Hypoxia imaging with the nitroimidazole ^{18}F-FAZA PET tracer: A comparison with OxyLite, EPR oximetry and ^{19}F-MRI relaxometry. *Radiother Oncol* 2012;105:29-35.
16. Caceci MS, Cacheris WP. Fitting curves to data: The simplex algorithm is the answer. *Byte* 1984;9:340-362.
17. Dunn TJ, Braun RD, Rhemus WE, et al. The effects of hyperoxic and hypercarbic gases on tumour blood flow. *Br J Cancer* 1999;80:117-126.
18. Colliez F, Neveu MA, Magat J, et al. Qualification of a noninvasive magnetic resonance imaging biomarker to assess tumor oxygenation. *Clin Cancer Res* 2014;20:5403-5411.
19. Renou JP, Kopp J, Valin C. Use of low resolution NMR for determining fat content in meat products. *Int J Food Sci Technol* 1985;20:23-29.
20. Edzes HT, Samulski ET. Cross relaxation and spin diffusion in the proton NMR or hydrated collagen. *Nature* 1977;265:521-523.
21. Zhang L, Wang L, Kao YT, et al. Mapping hydration dynamics around a protein surface. *Proc Natl Acad Sci U S A* 2007;104:18461-18466.
22. Beeman SC, Shui YB, Perez-Torres CJ, et al. O_2-sensitive MRI distinguishes brain tumor versus radiation necrosis in murine models. *Magn Reson Med* 2016;75:2442-2447.
23. O'Connor JP, Rose CJ, Waterton JC, et al. Imaging intratumor heterogeneity: Role in therapy response, resistance, and clinical outcome. *Clin Cancer Res* 2015;21:249-257.
24. Baudelet C, Gallez B. How does blood oxygen level-dependent (BOLD) contrast correlate with oxygen partial pressure (pO_2) inside tumors? *Magn Reson Med* 2002;48:980-986.
25. Rijpkema M, Kaanders JH, Joosten FB, et al. Effects of breathing a hyperoxic hypercapnic gas mixture on blood oxygenation and vascularity of head-and-neck tumors as measured by magnetic resonance imaging. *Int J Radiat Oncol Biol Phys* 2002;53:1185-1191.
26. Griffiths JR, Taylor NJ, Howe FA, et al. The response of human tumors to carbogen breathing, monitored by gradient-recalled echo magnetic resonance imaging. *Int J Radiat Oncol Biol Phys* 1997;39:697-701.
27. Hallac RR, Ding Y, Yuan Q, et al. Oxygenation in cervical cancer and normal uterine cervix assessed using blood oxygenation level-dependent (BOLD) MRI at 3T. *NMR Biomed* 2012;25:1321-1330.
28. Linnik IV, Scott ML, Holliday KF, et al. Noninvasive tumor hypoxia measurement using magnetic resonance imaging in murine U87 glioma xenografts and in patients with glioblastoma. *Magn Reson Med* 2014;71:1854-1862.